THE JOURNAL OF BIOLOGICAL CHEMISTRY VOL. 283, NO. 20, pp. 13973–13982, May 16, 2008
© 2008 by The American Society for Biochemistry and Molecular Biology, Inc. Printed in the U.S.A.

Cytochrome bc_1-c_y Fusion Complexes Reveal the Distance Constraints for Functional Electron Transfer Between Photosynthesis Components*

Received for publication, January 4, 2008, and in revised form, March 14, 2008 Published, JBC Papers in Press, March 14, 2008, DOI 10.1074/jbc.M800091200

Dong-Woo Lee[‡], Yavuz Öztürk[‡§], Artur Osyczka[¶1], Jason W. Cooley[‡2], and Fevzi Daldal[‡3]

From the [‡]Department of Biology, the Plant Science Institute and the [¶]Department of Biochemistry and Biophysics, University of Pennsylvania, Philadelphia, Pennsylvania 19104 and the [§]TUBITAK-Marmara Research Centre, Genetic Engineering and Biotechnology Institute, Gebze, Kocaeli 41470, Turkey

Photosynthetic (Ps) growth of purple non-sulfur bacteria such as *Rhodobacter capsulatus* depends on the cyclic electron transfer (ET) between the ubihydroquinone (QH_2): cytochrome (cyt) *c* oxidoreductases (cyt bc_1 complex), and the photochemical reaction centers (RC), mediated by either a membrane-bound (cyt c_y) or a freely diffusible (cyt c_2) electron carrier. Previously, we constructed a functional cyt bc_1-c_y fusion complex that supported Ps growth solely relying on membrane-confined ET (Lee, D.-W., Ozturk, Y., Mamedova, A., Osyczka, A., Cooley, J. W., and Daldal, F. (2006) *Biochim. Biophys. Acta* 1757, 346–352). In this work, we further characterized this cyt bc_1-c_y fusion complex, and used its derivatives with shorter cyt c_y linkers as "molecular rulers" to probe the distances separating the Ps components. Comparison of the physicochemical properties of both membrane-embedded and purified cyt bc_1-c_y fusion complexes established that these enzymes were matured and assembled properly. Light-activated, time-resolved kinetic spectroscopy analyses revealed that their variants with shorter cyt c_y linkers exhibited fast, native-like ET rates to the RC via the cyt bc_1. However, shortening the length of the cyt c_y linker decreased drastically this electronic coupling between the cyt bc_1-c_y fusion complexes and the RC, thereby limiting Ps growth. The shortest and still functional cyt c_y linker was about 45 amino acids long, showing that the minimal distance allowed between the cyt bc_1-c_y fusion complexes and the RC and their surrounding light harvesting proteins was very short. These findings support the notion that membrane-bound Ps components form large, active structural complexes that are "hardwired" for cyclic ET.

Gram-negative, purple, non-sulfur, facultative phototrophic α-proteobacteria of *Rhodobacter* species provide excellent model systems for studying photosynthetic (Ps)[4] and respiratory electron transfer (ET) chains (1–4). Among them, *Rhodobacter capsulatus* uses both a freely diffusible and a membrane-anchored cytochrome (cyt) (c_2 and c_y, respectively) electron carrier between the ubihydroquinone (QH_2):cyt *c* oxidoreductase (cyt bc_1 complex) and either the photochemical reaction center (RC) or the cbb_3-type cyt *c* oxidase (C_{ox}) under Ps or respiratory growth conditions, respectively (5–7). In contrast, the closely related *Rhodobacter sphaeroides* relies exclusively on the soluble cyt c_2 for its Ps growth (8), even though it has a membrane-bound cyt c_y that is functional only under respiratory growth conditions (9). *R. capsulatus* cyt c_y is 199 amino acids long, with its NH_2-terminal 28 residues corresponding to an unprocessed signal sequence-like membrane anchor and COOH-terminal 100 residues (Thr^{99} to Arg^{199}) to a monoheme cyt *c* domain (10). The remaining 70-residues (Asn^{28} to Thr^{98}) long Ala and Pro-rich region of cyt c_y forms a linker attaching the cyt *c* domain to the membrane anchor and allowing its observed mobility (11). Noticeably, the linker of *R. capsulatus* cyt c_y is markedly longer than that of *R. sphaeroides* and other non-Ps bacterial cyt c_y (Fig. 1*A*). A seminal finding was that *R. sphaeroides* mutants lacking cyt c_2 can be complemented for Ps growth by *R. capsulatus* cyt c_y (12), pointing out that the cyt c_y linker length might be critical for its electron carrier function during Ps cyclic ET.

Earlier studies, regarding the rate of ET mediated by cyt c_y from the cyt bc_1 complex to the RC, and the correlative presence of the cyt bc_1 complex with cyt c_y in membranes (7, 13), suggested that these proteins must be in close proximity to one another and to the RC and its light harvesting (LH) complexes. Occurrence of larger, nontransient macromolecular structures, ensuring efficient substrate channeling, catalytic enhancement, and sequestration of reactive intermediates during electron transport have been proposed to occur in membranes of purple bacteria (14), plants (15), and mitochondria (16). However, as the membrane-embedded components can diffuse independently from one another within lipid bilayers, differentiating between static "hardwired" electron transport complexes from those undergoing random collisions (17) is difficult to document in Ps membranes (18). In the accompanying work (38), we have demonstrated by creating soluble variants of cyt c_y (cyt

* This work was supported, in whole or in part, by National Institutes of Health Grant GM38237. This work was also supported by Department of Energy Grant ER9120053. The costs of publication of this article were defrayed in part by the payment of page charges. This article must therefore be hereby marked "*advertisement*" in accordance with 18 U.S.C. Section 1734 solely to indicate this fact.

[1] Present address: Dept. of Biophysics, Faculty of Biochemistry, Biophysics and Biotechnology, Jagiellonian University, Krakow, Poland.

[2] Present address: Dept. of Chemistry, University of Missouri, Columbia, MO 65211.

[3] To whom correspondence should be addressed. Tel.: 215-898-4394; Fax: 215-898-8780; E-mail: fdaldal@sas.upenn.edu.

[4] The abbreviations used are: Ps, photosynthetic; cyt, cytochrome; RC, photochemical reaction center; LH, light harvesting; ET, electron transfer; TMBZ, 3,3′,5,5′-tetramethylbenzidine; Q/QH_2, quinone/hydroquinone pool; NQ, 1,2-naphthoquinone; HNQ, 2-hydroxy-1,4-naphthoquinone; DDM, dodecyl maltoside; MOPS, 4-morpholinepropanesulfonic acid; CV, column volume.

S-c_y) that this electron carrier needs not be membrane anchored to support Ps growth of *R. capsulatus*. In this work, we have exploited the functional cyt bc_1-c_y fusion complex that we constructed earlier by fusing genetically cyt c_y to the cyt bc_1 complex (19) to probe the physical proximities of the Ps components to one another in *R. capsulatus*. We surmised that if the native length of the cyt c_y linker is optimized for efficient electronic coupling across the distance between the cyt bc_1 complex and the RC, then progressively shortening it might divulge the minimal distances separating these physiological partners in Ps membranes. Characterization of the physicochemical properties of both membrane-embedded and highly purified cyt bc_1-c_y fusion complex variants indicate that the shortest functional cyt c_y linker is about 45 residues long. This short linker still insures rapid ET from the cyt bc_1 to the RC, but exhibits decreased electronic coupling to the RC, thereby limiting cyclic ET and Ps growth. Thus, Ps cyclic ET components appear to be tightly packed together, forming membrane-embedded large structural complexes.

EXPERIMENTAL PROCEDURES

Bacterial Strains and Growth Conditions—Bacterial strains and plasmids used in this study are listed in Table 1. *R. capsulatus* strains were grown at 35 °C in mineral-peptone-yeast extract-enriched media (MPYE) supplemented with antibiotics as needed (10, 2.5, and 10 μg/ml kanamycin, tetracycline, and spectinomycin, respectively) under either semiaerobic/dark (respiratory), or photoheterotrophic/light (Ps) conditions using anaerobic jars and H_2 + CO_2 generating gas packs (BD Biosciences), as described previously (20). Ps growth curves were obtained using screw-cap tubes, incubated at 35 °C in an aquarium filled with water and illuminated by tungsten (Lumiline, Sylvania) lamps at an intensity of 150 μE/m^2/s. Culture turbidity was monitored with a Klett-Summerson photometer equipped with a red (number 66) filter as described (21).

Molecular Genetic Techniques—PCR amplification of a 0.7-kb carboxyl-terminal FLAG epitope-tagged allele of *cycY* on plasmid pHM7 (10) using mutagenic primers YO5EcoRV (5′-GCCGGGGGATATCTGCTCGTCAAGACGCACATC-3′) and YO6HindIII (5′-GCCGGGGCAAGCTTGCAAAGAT-GTGAGGGC-3′) replaced the initiating methionine (ATG) of *cycY* with leucine (CTG). This PCR product was then digested with EcoRV and HindIII restriction enzymes and ligated into the StuI and HindIII sites of plasmid pMTS1 (20), to yield pYO37 containing a *petABC*::*cycY* fusion without the stop codon (TGA) of *petC* (cyt c_1). The BamHI-HindIII fragment of pYO37 was transferred into the same sites of the broad host range plasmid pRK415, yielding pYO38 (Table 1). Similarly, two additional in-frame deletion derivatives of pYO38 (Δ19 and Δ24 in the linker region of cyt c_y) of the *cycY*-FLAG fusion were obtained by appropriate PCR amplification of the 0.7-kb carboxyl-terminal FLAG epitope-tagged version of *cycY*, yielding pYO32 (*petABC*::*cycY*-FLAG-Δ19) and pYO29 (*petABC*::*cycY*-FLAG-Δ24), respectively, and transferred to the BamHI-HindIII sites of pRK415 to yield pYO33 and pYO30, respectively. All constructs were subsequently verified by DNA sequencing.

A Δ(*petABC*::gen) insertion-deletion allele was constructed by replacing the 2.4-kb ApaLI-StuI fragment of *petABC* in plasmid pMTS1 with the 1.2-kb HindIII-BamHI fragment containing the gentamycin resistance gene by blunt end ligation, yielding pYO34. This Δ(*petABC*::gen) allele was then transferred using Gene Transfer Agent into the chromosome of *R. capsulatus* strain FJ2 (Δ*cycA*, Δ*cycY*) (5) to yield the triple mutant YO2, lacking both the cyt bc_1 complex and electron carrier cyts c_2 and c_y.

Biochemical Techniques—Intracytoplasmic (chromatophore) membranes were prepared as described previously (19), except where noted 1 mM ϵ-aminocaproic acid and 100 mM EDTA were added to minimize proteolysis following cell disruption. The *R. capsulatus* cyt bc_1 complex was purified as described previously (22). Protein concentrations were determined using the bicinchoninic acid method (23) with bovine serum albumin as a standard. SDS-PAGE (15%) were run as described in Ref. 24, and prior to loading, samples were solubilized in 62.5 mM Tris-HCl (pH 6.8), 2% SDS, 0.1 M dithiothreitol, 25% glycerol, and 0.01% bromphenol blue with subsequent incubation at 60 °C for 10 min. Cytochromes *c* were visualized by their heme peroxidase activities using 3,3′,5,5′-tetramethylbenzidine (TMBZ) and H_2O_2 according to Thomas *et al.* (25).

Spectroscopic Techniques—Optical spectra were recorded on a PerkinElmer UV-visible spectrophotometer Lambda 20. Absorption difference spectra for the *c*- and *b*-type cytochromes were obtained using chromatophore membranes (0.3 mg of total protein/ml), oxidized by adding a crystal of potassium ferricyanide, and reduced by a few grains of either solid sodium ascorbate or sodium dithionite, as appropriate. Time-resolved, light-activated kinetic spectroscopy was performed on a dual wavelength kinetic spectrophotometer with chromatophore membranes resuspended in 50 mM MOPS buffer containing 100 mM KCl (pH 7.0) in the presence of the following redox mediators (with their respective midpoint redox potential, $E_{m,7}$): 100 μM ferricyanide (430 mV), 8 μM 2,3,5,6-tetramethyl-*p*-phenylenediamine (260 mV), 6 μM 1,2-naphthoquinone (NQ, 145 mV), 1 μM phenazine methosulfate (80 mV), 1 μM phenazine ethosulfate (50 mV), 6 μM 2-hydroxy-1,4-naphthoquinone (HNQ, −145 mV), 6 μM benzyl viologen (−359 mV), and a membrane potential uncoupler (2.5 μM valinomycin), as described (26). The amount of chromatophore membranes used in each assay was normalized to the RC content, as determined by measuring the flash-induced optical absorbance difference between 605 and 540 nm at an E_h of 380 mV, and using an extinction coefficient of 29.8 mM^{-1} cm^{-1}. Transient cyt *c* re-reduction and cyt *b* reduction kinetics at an ambient potential of 100 mV, initiated by a short saturating flash (~8 μs) from a xenon lamp were followed at 550–540 and 560–570 nm, respectively. Antimycin, myxothiazol, and stigmatellin were used as indicated at 5, 5, and 1 μM, respectively.

Optical potentiometric titrations were performed with the purified cyt bc_1-c_y fusion complex (0.1 mg/ml) in 50 mM MOPS buffer (100 mM KCl, pH 7.0) with the following mediators: 20 μM tetrachlorohydroquinone (350 mV), 20 μM 2,3,5,6-tetramethyl-*p*-phenylenediamine, 20 μM 1,2-naphthoquinone 4-sulfonate (210 mV), 20 μM NQ, 10 μM phenazine methosulfate, 10 μM phenazine ethosulfate, 40 μM

duroquinone (5 mV), 20 μM pyocyanine (PCN, −34 mV), 6 μM indigotrisulfonate (−90 mV), 20 μM HNQ, 20 μM anthroquinone 2-sulfonate (−225 mV). The optical changes that accompanied the E_h changes were recorded in the α-band region (500 to 600 nm), and the E_m values were determined by fitting the normalized absorption data to a single component $n = 1$ Nernst equation. EPR spectroscopy was performed at sample temperatures of 10 or 20 K using a Bruker ESP 300E spectrometer (Bruker Biosciences), fitted with an Oxford instruments ESR-9 helium cryostat (Oxford Instrumentation Inc.). Spectrometer settings were as indicated in the appropriate figure legends.

Purification of the Cyt bc_1-c_y Fusion Complex—The *R. capsulatus* cyt bc_1-c_y fusion complex was purified using pYO38/YO2. Chromatophore membranes (5.9 g wet weight) were obtained from frozen washed cells (81 g wet weight) after two passages through a French pressure cell and collected by ultracentrifugation (20). Chromatophore pellets were resuspended to a final protein concentration of 18 mg/ml in 50 mM phosphate buffer (pH 8.0) containing 7.2 mM NaCl, 20% glycerol, 1 mM phenylmethylsulfonyl fluoride, 100 mM EDTA, 10 protease inhibitor mixture tablets (Roche Applied Science) and 1 mM ϵ-aminocaproic acid. Dodecyl maltoside (DDM, 20% w/v stock solution) was added dropwise to this suspension to a final concentration of 1 mg of DDM/mg of total proteins. The mixture was stirred gently for 1 h at 4 °C, and then ultracentrifuged (120,000 × *g* for 2 h) to eliminate non-dispersed membranes. The supernatant was loaded onto a Q-Sepharose ff column (2.6 × 32 cm) pre-equilibrated with 50 mM phosphate buffer (pH 8.0) containing 20% glycerol, 0.01% (w/v) DDM, and 7.2 mM NaCl (Buffer A). The column was washed with 5 to 6 column volumes (CVs) of Buffer A containing 400 mM NaCl, and then the remaining photosynthetic pigments were washed with 3 to 4 CVs of the same buffer containing 0.05% (w/v) DDM until a red band on top of the column became visible. The adsorbed cyt bc_1-c_y fusion proteins were eluted with 4 CVs of a linear 400–800 mM NaCl gradient in the presence of 0.05% (w/v) DDM. Fractions were monitored for their absorption at 280 and 420 nm, and 500 to 600 nm for their dithionite-reduced *minus* ferricyanide-oxidized optical difference spectra, and those containing the highest concentrations of *c*-type and *b*-type cytochromes were pooled, concentrated using an Amicon Diaflo apparatus equipped with a PM30 membrane. The concentrated sample (~33 ml) was passed twice through an anti-FLAG M2 affinity column (5 ml), pre-equilibrated with 10 CVs of 50 mM phosphate buffer (pH 8.0) containing 150 mM NaCl and 0.01% (w/v) DDM. The column was then washed with 20 CVs of the same buffer, and eluted with 6 CVs of 100 mM glycine-HCl buffer (pH 3.5) containing 0.01% (w/v) DDM. Eluents were collected into vials containing 1 M Tris-HCl buffer (pH 8.0) to a final concentration of 50 mM. Fractions containing the cyt bc_1-c_y fusion complex were pooled, buffer exchanged with 50 mM phosphate buffer (pH 8.0) containing 0.01% (w/v) DDM using Amicon Ultra (50,000 M_r cut off) centrifugal filter devices (Millipore Co., Ireland), and stored at −80 °C in the presence of 20% glycerol until further use.

RESULTS

Design of the Cyt bc_1-c_y Fusion Complexes with Shorter Cyt c_y Linker Lengths—The availability of a functional cyt bc_1-c_y fusion complex (19) allowed us to probe whether the cyt c_y linker could be used as a "molecular ruler" to estimate the distances between the Ps ET components. Comparison of *R. capsulatus* cyt c_y with its counterparts from other species indicated that the cyt *c* domain is highly similar to that from *Silicibacter pomeroyi* (71%), *Paracoccus denitrificans* (70%), and *R. sphaeroides* (65%). On the other hand, the linker regions of *P. denitrificans*, *R. sphaeroides*, and *S. pomeroyi* are about 20 to 30 residues shorter than that of *R. capsulatus* (Fig. 1*A*). Generation of computer-assisted hypothetical three-dimensional structures of the cyt bc_1-c_y fusion complexes with shorter linkers directed us to the region between amino acids 65 and 90 of cyt c_y to mimic its non-functional variants as Ps electron carriers (Fig. 1*B*). Considering that the *R. sphaeroides* cyt c_y linker is 26 amino acids shorter than its *R. capsulatus* counterpart, plasmids pYO30 (with a 24-amino acid long deletion between positions Ala^{63} and Pro^{88} of cyt c_y) (Δ24-c_y) and pYO33 (with a 19-amino acid long deletion between the positions Ala^{67} and Pro^{88} of cyt c_y) (Δ19-c_y) were constructed to determine the Ps ET of each electron carrier (Table 1).

Phenotypic Characterization of R. capsulatus Strains Harboring Cyt bc_1-c_y Fusion Complex Variants with Shorter Cyt c_y Linkers—Plasmids pYO30 (Δ24-c_y) and pYO33 (Δ19-c_y) were introduced into the *R. capsulatus* mutant YO2 (lacking the cyts bc_1, c_2, and c_y), and the Ps growth abilities of the resulting strains were examined (Fig. 2*A*). On enriched MPYE medium under Ps conditions, *R. capsulatus* strain pMTS1/MT-RBC1 overproducing cyt bc_1 complex, MT-G4/S4 lacking the cyt c_2, and pYO38/YO2 harboring an intact cyt bc_1-c_y fusion complex exhibited doubling times of about 192, 216, and 300 min, respectively (Fig. 2*A*). However, under similar conditions, pYO33/YO2 (Δ24-c_y) and pYO30/YO2 (Δ19-c_y) grew markedly slower than pYO38/YO2 (native-c_y) (756 and 498 *versus* 300 min, respectively). As the mutant YO2 cannot be complemented for Ps growth by either the cyt bc_1 complex or cyt c_y alone, the data indicated that the cyt bc_1-c_y fusion complexes with shorter cyt c_y linkers provided both the oxidoreductase and electron carrier functions required for Ps growth. However, the slower growth rates suggested that shortening the cyt c_y linker hampered the growth abilities of PS.

Prosthetic Group Insertion, Enzymatic Activity, and Subunit Assembly of the Cyt bc_1-c_y Fusion Complexes—As the slower Ps growth might also be attributed to decreased amounts of cyt bc_1-c_y fusion complexes, chromatophore membranes of appropriate strains were examined by TMBZ/SDS-PAGE analyses (Fig. 2*B*). Typical membrane-associated *c*-type cytochrome profiles comprised of the cyts c_p (32 kDa), c_1 (30 kDa), c_y (29 kDa), and c_o (28 kDa) were observed for pMTS1/MT-RBC1 and MT-G4/S4, whereas the YO2-derived samples contained only cyts c_p and c_o (both subunits of C_{ox}) as expected. On the other hand, pYO38/YO2, pYO33/YO2, and pYO30/YO2 harboring cyt bc_1-c_y fusion complexes with shorter cyt c_y linkers had both

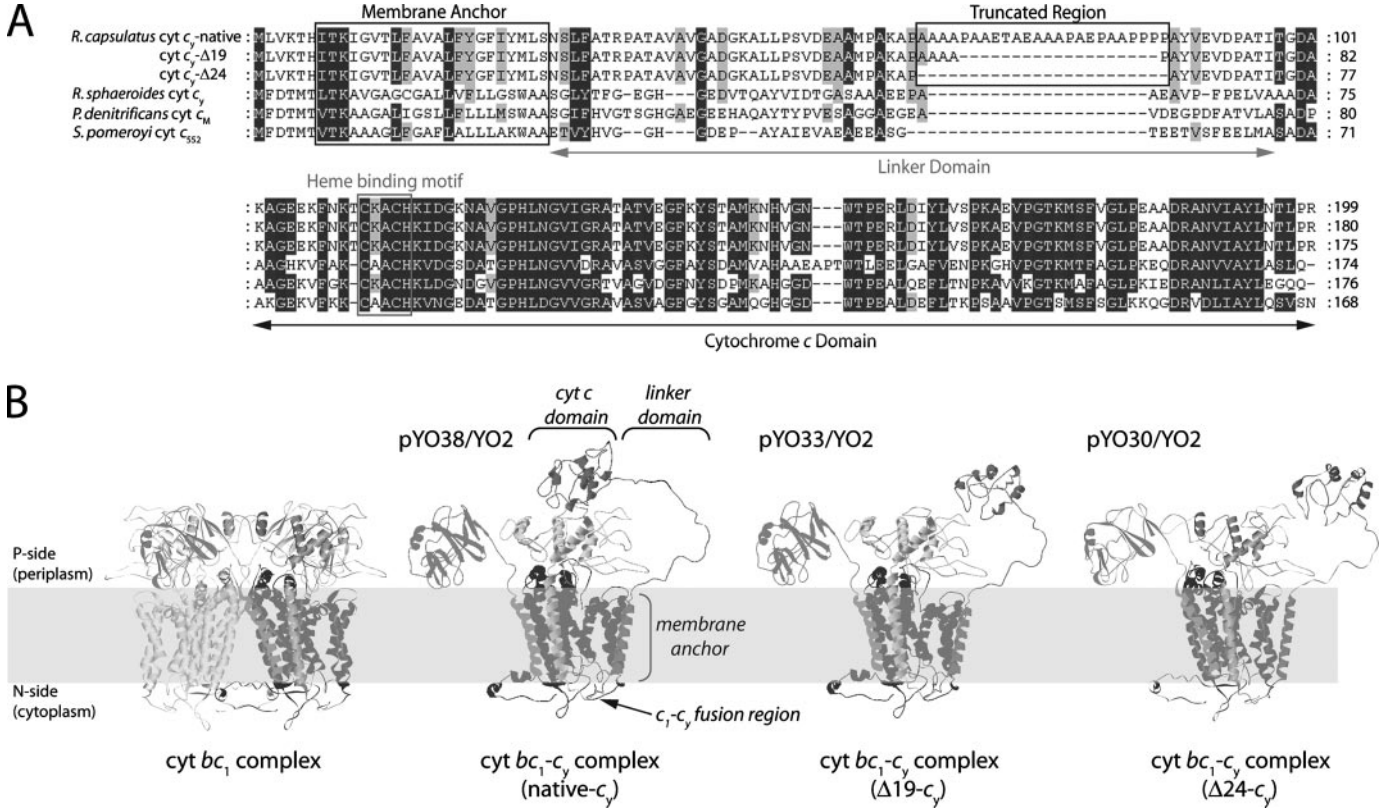

FIGURE 1. *A*, amino acid sequence alignments of *R. capsulatus* cyt c_y and its shorter linker variants with its homologues in other species, *R. capsulatus* cyt c_y (native linker) (CAA79860); *R. capsulaturs* cyt c_y (Δ19); *R. capsulatus* cyt c_y (Δ24); *R. sphaeroides* cyt c_y (AAC26877); *P. denitrificans* cyt c_M (CAA49830); and *S. pomeroyi* DSS-3 cyt c_{552} (AAV96763). *B*, hypothetical three-dimensional structural models of the *R. capsulatus* cyt bc_1-c_y fusion complex and its shorter linker derivatives. The cyt *c* domain of *R. capsulatus* c_y was modeled using SWISS-MODEL, and the overall structures were visualized using the *R. capsulatus* cyt bc_1 (Protein Data Bank 1ZRT) and yeast cyt bc_1:cyt *c* co-crystal (PDB 1NTK) structures.

TABLE 1

***R. capsulatus* strains used**

Strain *R. capsulatus*	Genotype	Phenotype	Ref.
MT-G4/S4	*crt*D121 Rif^R, Δ(*cycA*::*kan*)	Cyt c_2^-, Kan^R, Ps$^+$	5
YO2	*crt*D121 Rif^R, Δ(*petABC*::*gen*), Δ(*cycA*::*kan*), Δ(*cycY*::*spe*)	Cyt c_2^-, cyt c_y^-, cyt bc_1^-, Gen ^{R}, Kan ^{R}, Spe ^{R}, Ps$^-$	19
pMTS1/MT-RBC1	MT-RBC1 strain (*crt*D121 Rif^R, Δ(*petABC*::*spe*), cyt bc_1^-, Spe^R, Ps-) with an expression plasmid carrying *petABC*	Cyt bc_1^+, Kan^R, Ps$^+$	37
pYO38/YO2	YO2 strain with an expression plasmid carrying *petABC*::*cycY*-FLAG (native cyt c_y)	Cyt bc_1-c_y^+, Tet^R, Ps$^+$	19
pYO33/YO2	YO2 strain with an expression plasmid carrying *petABC*::*cycY* (ΔAla^{67}-Pro^{87})-FLAG	Cyt bc_1-c_y^+ (Δ19 amino acid), Tet^R, Ps$^+$	This work
pYO30/YO2	YO2 strain with an expression plasmid carrying *petABC*::*cycY* (ΔAla^{63}-Pro^{88})-FLAG	Cyt bc_1-c_y^+ (Δ24 amino acid), Tet^R, Ps$^+$	This work

cyts c_1 and c_y bands replaced by a single peroxidase-active band at 61, 59, and 58 kDa, respectively, corresponding to their cyt c_1-c_y fusion subunits.

Steady-state enzymatic activities of the cyt bc_1 complexes were also assayed by measuring DBH_2-dependent reduction of horse heart cyt *c* (Fig. 2*C*). pYO38/YO2, pYO33/YO2, and pYO30/YO2 harboring cyt bc_1-c_y fusion complexes with different lengths of cyt c_y linkers showed very similar levels of DBH_2:cyt *c* reductase activities as compared with that of the pMTS1/MT-RBC1 overproducing a native cyt bc_1 complex. Therefore, neither fusing cyt c_y to cyt c_1, nor changing the length of the cyt c_y linker region significantly affected the cyt bc_1 complex enzymatic activity of various cyt bc_1-c_y fusion complexes with different cyt c_y linker lengths.

The presence of *b*-type cyts and cyts *c* to *b* ratios for all strains were also determined using optical difference spectroscopy to assess the relative amounts of the cyt bc_1 complexes. Changes in the amounts of the *c*-type (α $peak_{max}$ at 551 nm, $\epsilon_{551-542}$ of 20 mM^{-1} cm^{-1}) and *b*-type (α $peak_{max}$ at 560 nm, $\epsilon_{560-574}$ of 28 mM^{-1} cm^{-1}) cytochromes were monitored after reduction by ascorbate and dithionite, respectively, of ferricyanide-oxidized chromatophore membranes from appropriate strains (Fig. 3). Strains pMTS1/MT-RBC1 and MT-G4/S4 exhibited cyt *c* to *b* ratios of ~1:2, whereas very small amounts of *c* or *b* peaks were detected in YO2. On the other hand, strains pYO38/YO2, pYO33/YO2, and pYO30/YO2 had similar amounts of *b*-type cytochromes with cyt *c* to *b* ratios of about 1:1 (Fig. 3). The data indicated that all strains contained

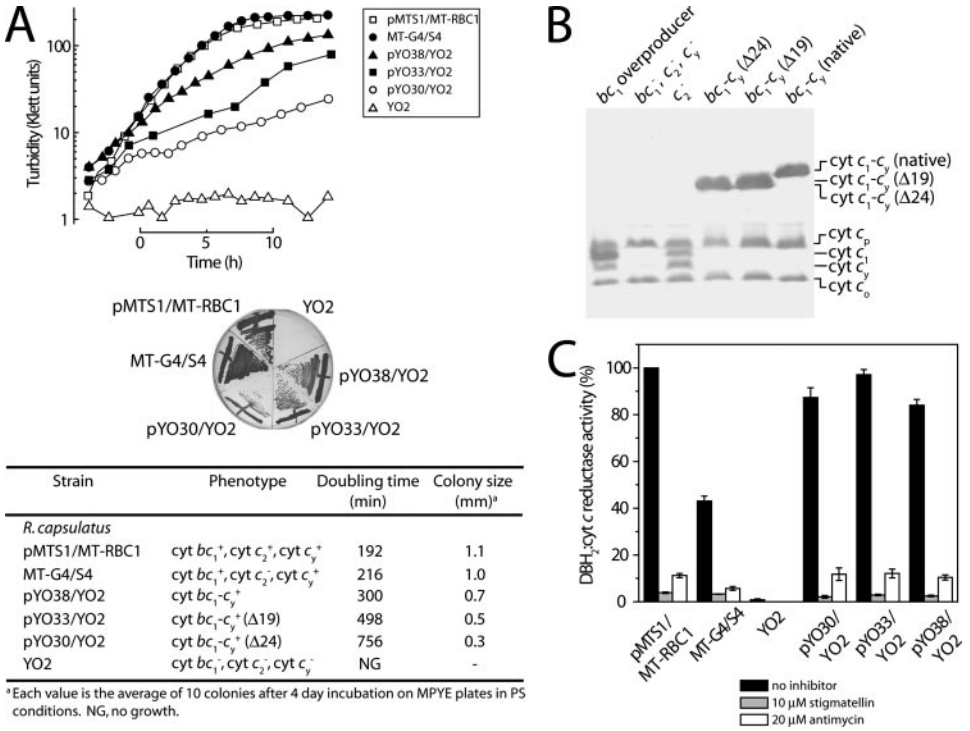

Strain	Phenotype	Doubling time (min)	Colony size (mm)[a]
R. capsulatus			
pMTS1/MT-RBC1	cyt bc_1^+, cyt c_2^+, cyt c_y^+	192	1.1
MT-G4/S4	cyt bc_1^+, cyt c_2^-, cyt c_y^+	216	1.0
pYO38/YO2	cyt bc_1-c_y^+	300	0.7
pYO33/YO2	cyt bc_1-c_y^+ (Δ19)	498	0.5
pYO30/YO2	cyt bc_1-c_y^+ (Δ24)	756	0.3
YO2	cyt bc_1^-, cyt c_2^-, cyt c_y^-	NG	-

[a] Each value is the average of 10 colonies after 4 day incubation on MPYE plates in PS conditions. NG, no growth.

FIGURE 2. *A*, photosynthetic growth properties on liquid and solid media (enriched MPYE) of various *R. capsulatus* strains (YO2 lacking the cyt bc_1, cyt c_y, and cyt c_2; pMTS1/MT-RBC1 overproducing the cyt bc_1 complex, MT-G4/S4 lacking the cyt c_2, and pYO38/YO2, pYO33/YO2, and pYO30/YO2 containing the cyt bc_1-c_y fusion complexes with the native 19 amino acids and 24-amino acid shorter cyt c_y linkers, respectively) were determined by monitoring the turbidity of the cultures, as described under "Experimental Procedures." *B*, the *c*-type cytochrome profiles of the same strains were revealed using chromatophore membranes (100 μg of total proteins per lane) and 15% SDS-PAGE/TMBZ analyses. *C*, DBH_2:cyt *c* reductase activities of chromatophore membranes (20 μg of total proteins) derived from the same strains described above were determined as in Atta-Asafo-Adjei and Daldal (20), in the absence (no inhibitor) or presence (10 μM stigmatellin or 20 μM antimycin), and for comparative purposes the steady-state enzymatic activities are represented as % of the overproduced native cyt bc_1 complex.

similar amounts of cyt bc_1-c_y fusion complexes regardless of the linker length of their cyt c_y. Furthermore, to confirm that the Fe-S subunits of fusion complexes had native-like physicochemical properties, EPR spectroscopy was used. Chromatophore membranes prepared from pYO38/YO2 exhibited the [2Fe-2S] cluster g_y and g_x signals of 1.891 and 1.806, respectively, which were identical to those seen with a native cyt bc_1 complex (*e.g.* MT-G4/S4) (Fig. 4*A*). Moreover, under appropriate conditions, the EPR signals with g_z values of 3.778 and 3.411 assigned to cyts b_L and b_H, respectively, were observed with the same membrane preparations (Fig. 4*B*). The overall data established that all cyt bc_1-c_y fusion complexes assembled similarly, and exhibited similar enzymatic activities, indicating that the slower growth rates observed with pYO33/YO2 and pYO30/YO2 could not be correlated with the amounts of fusion complexes.

Purification and Characterization of Purified Cyt bc_1-c_y Fusion Complexes—Purification of cyt bc_1-c_y fusion complexes was pursued to establish that they existed as intact physical entities in the membranes. Earlier, we partially purified the cyt bc_1-c_y fusion complex (19) using the procedure described by Valkova-Valchanova *et al.* (22). However, as detailed characterization required purer samples, we developed a new procedure. About 8 mg of purified cyt bc_1-c_y fusion complex was obtained starting with about 2.5 g of chromatophore membranes derived from 97 g (wet weight) of cells, followed by detergent solubilization, Q-Sepharose ff ion-exchange and FLAG affinity column chromatographies (Table 2). The final preparations of the cyt bc_1-c_y fusion complex contained less than 5% of Ps pigments associated with the LH complexes, as estimated by optical spectra (data not shown). The purified cyt bc_1-c_y fusion complex was highly active, reducing horse heart cyt *c* as an electron acceptor with decylhydroquinone as an electron donor ("Experimental Procedures"). Its specific activity (about 27.2 nmol/mg of protein/min under the assay conditions used) was comparable with that of the purified cyt bc_1 complex (41.0 nmol/mg of protein/min) (22). Optical difference spectra indicated that the purified cyt bc_1-c_y fusion complex had a cyt *b* to *c* ratio of ~1:1, similar to that seen in chromatophore membranes from pYO38/YO2 (data not shown). Potentiometric redox equilibrium titration of the heme groups of the cyt c_1-c_y fusion subunit in the presence of 100 mM KCl at pH 7.0 indicated a single component with an $E_{m,7}$ value of +336 mV (Fig. 5*B*). Considering that this subunit is a diheme *c*-type cyt (cyts c_1 and c_y of $E_{m,7}$ of 320 and 365 mV, respectively (10, 27), the data suggested that the two hemes were in rapid equilibrium with each other, with a mean $E_{m,7}$ value high enough to convey electrons efficiently from the cyt bc_1 complex to the RC.

SDS-PAGE analysis of purified cyt bc_1-c_y fusion complex showed three major bands with 61, 41, and 24 kDa, assigned to the cyt c_1-c_y, cyt *b*, and the Fe-S protein subunits, respectively, by TMBZ staining and immunoblot analyses with specific monoclonal antibodies (Fig. 5*A*). Additional bands of higher M_r seen with the cyt bc_1-c_y fusion complexes were attributed to their aggregated forms, based on TMBZ staining and immunoblot data, as they were also seen with native cyt bc_1 complexes (27). Finally the non-stoichiometric band running between the cyt *b* and Fe-S protein subunits, and detected weakly by cyt c_1-specific antibodies, in FLAG affinity purified samples reflected degradation products of the cyt c_1-c_y fusion subunit. The oligomeric state of purified cyt bc_1-c_y fusion complex was determined by size exclusion chromatography using an analytical grade Superose 6 HR 10/30 (GE Healthcare Inc.) column calibrated with high molecular weight standard markers in the presence of 0.05% (w/v) DDM and 150 mM NaCl (Fig. 5*B*). Under these conditions, the purified cyt bc_1 complex runs as one major peak around 240 kDa (estimated to correspond to its dimeric form), whereas the purified cyt bc_1-c_y fusion complex

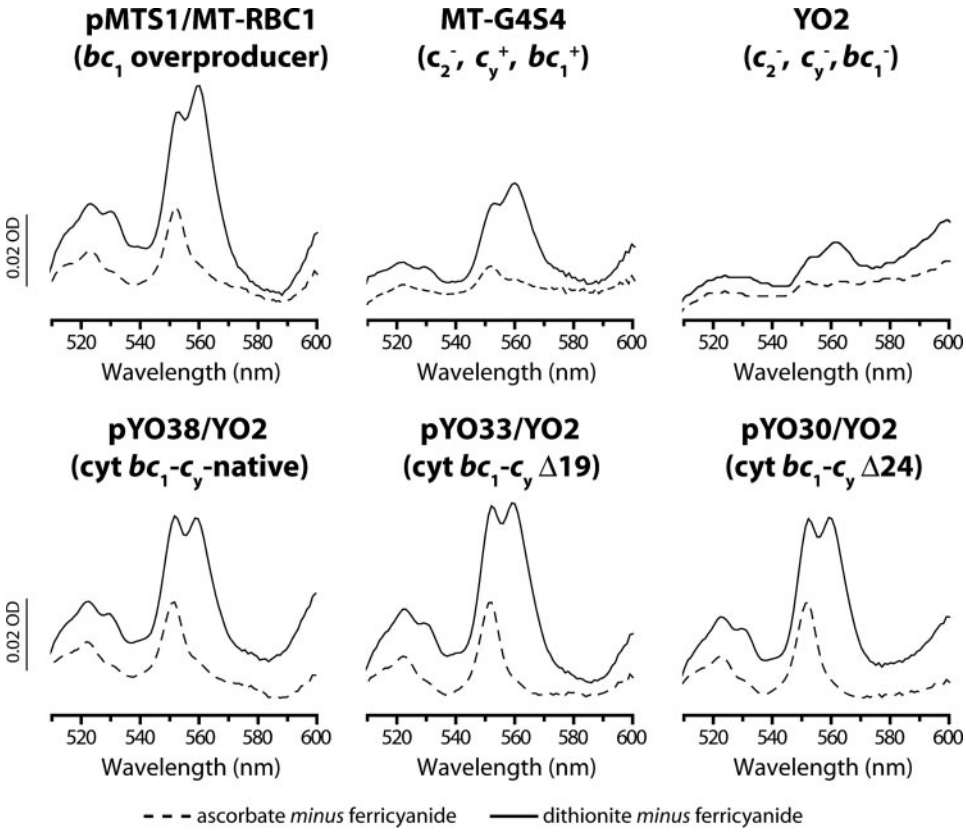

FIGURE 3. **Reduced *minus* oxidized optical difference spectra of *b*-type and *c*-type cytochromes in chromatophore membranes (0.4 mg of total proteins) from various *R. capsulatus* strains.** Strains were as described in the legend to Fig. 2, and grown on enriched MPYE medium by respiration.

exhibited two major peaks at about 417 and 257 kDa, respectively. Immunoblot analyses with subunit-specific antibodies showed that both peaks had homogeneous constituents, suggesting that purified cyt bc_1-c_y fusion complexes consisted of a mixture of tetrameric and dimeric forms under the conditions used.

Light-activated Cyt b Reduction and Cyt c Re-reduction Kinetics—A major aim being to probe the extent of ET from the cyt bc_1-c_y fusion complexes with shorter cyt c_y linkers to the RC *in situ*, appropriate strains were examined using light-activated, time-resolved optical spectroscopy (Fig. 6). In all cases, chromatophore membranes were normalized to the same amounts of photooxidized RC by measuring the absorbance changes at 605-540 nm at an E_h of 380 mV after a train of 10 saturating actinic flashes spaced 50 ms apart. Transient cyt *b* reduction and cyt *c* re-reduction kinetics, initiated by rapid (microsecond time scale) light activation of the RC, were monitored on the millisecond time scale, at an ambient redox potential E_h of 100 mV. At this E_h, the membrane Q pool contains Q and QH_2, and the RC as well as cyts *c*, and the [2Fe-2S] cluster of the Fe-S protein subunits of cyt bc_1 or the cyt bc_1-c_y fusion complexes are fully reduced. First, light-induced time-resolved single turnover cyt *b* reduction kinetics were examined at 560–570 nm, in the presence and absence of antimycin A as a specific cyt bc_1 complex Q_i site inhibitor. In MT-G4/S4, which has only cyt c_y as the sole electron carrier between the cyt bc_1 complex and the RC, and in pYO38/YO2 producing a cyt bc_1-c_y fusion complex with a native cyt c_y linker, cyt *b* was reduced by oxidation of a QH_2 via the Q_o site, and immediately re-oxidized by Q bound at the Q_i site with an expected rate faster than the available time resolution. However, in the presence of antimycin A (2 μM), cyt *b* oxidation was abolished to reveal the light-induced transient reduction phase (Fig. 6, *top row*). In the case of pYO33/YO2 (Δ19-c_y) and pYO30/YO2 (Δ24-c_y) with shorter cyt c_y linkers, fast cyt *b* oxidation/reduction rates were quasi-similar to those seen with MT-G4/S4 and pYO38/YO2, but the amplitudes of these changes (per RC) were significantly smaller (Fig. 6, *top row*). As similar amounts of cyt bc_1-c_y fusions complexes were present in all strains tested (Figs. 2 and 3) the smaller cyt *b* reduction amplitudes cannot be interpreted as lower amounts of these complexes in the membranes.

The cyt *c* oxidation/re-reduction kinetics exhibited by the cyt bc_1 complexes were subsequently examined using the specific Q_o site inhibitors myxothiazol and stigmatellin to probe ET to the RC. Myxothiazol blocks cyt *c* re-reduction by displacing QH_2 without immobilizing the Fe-S protein, whereas stigmatellin not only displaces QH_2 but also immobilizes the Fe-S protein to block ET to the c_1 heme as well. In the presence of stigmatellin, MT-G4/S4 and pYO38/YO2 showed typical cyt *c* oxidation without any cyt *c* re-reduction (Fig. 6, *bottom row*), due to the absence of ET from the Fe-S protein subunit to the cyt c_1 heme. In the presence of myxothiazol, cyt *c* re-reduction reached about half of the amplitude seen in the presence of stigmatellin (*i.e.* full oxidation), revealing the pre-flash, chemically derived electron localized in the Fe-S protein despite the absence of QH_2 oxidation at the Q_o site (Fig. 6, *bottom row*) (see *e.g.* Refs. 28 and 29 for a detailed explanation of these ET kinetics). Cyt *c* re-reduction kinetics exhibited by pYO33/YO2 (Δ19-c_y) and pYO30/YO2 (Δ24-c_y) were quasi-similar to those seen with MT-G4/S4 and pYO38/YO2 (native-c_y) in the presence and absence of the Q_o site inhibitors. However, in the presence of shorter cyt c_y linkers, significant differences in the cyt *c* oxidation/re-reduction amplitudes were observed. These amplitude decreases could not reflect lower amounts of the cyt bc_1-c_y fusion complexes with shorter cyt c_y linkers in the strains examined (Figs. 2 and 3). Thus, they indicated decreased electronic couplings to the RC, revealing the limits of their physical abilities to reach and convey electrons to the photooxidized RCs (Fig. 6). Comparative kinetic data indicated that a cyt c_y linker of about 45 amino acids long (*i.e.* Δ24-c_y) seems to be the shortest one able to sustain cyclic ET and Ps growth of *R. capsulatus*.

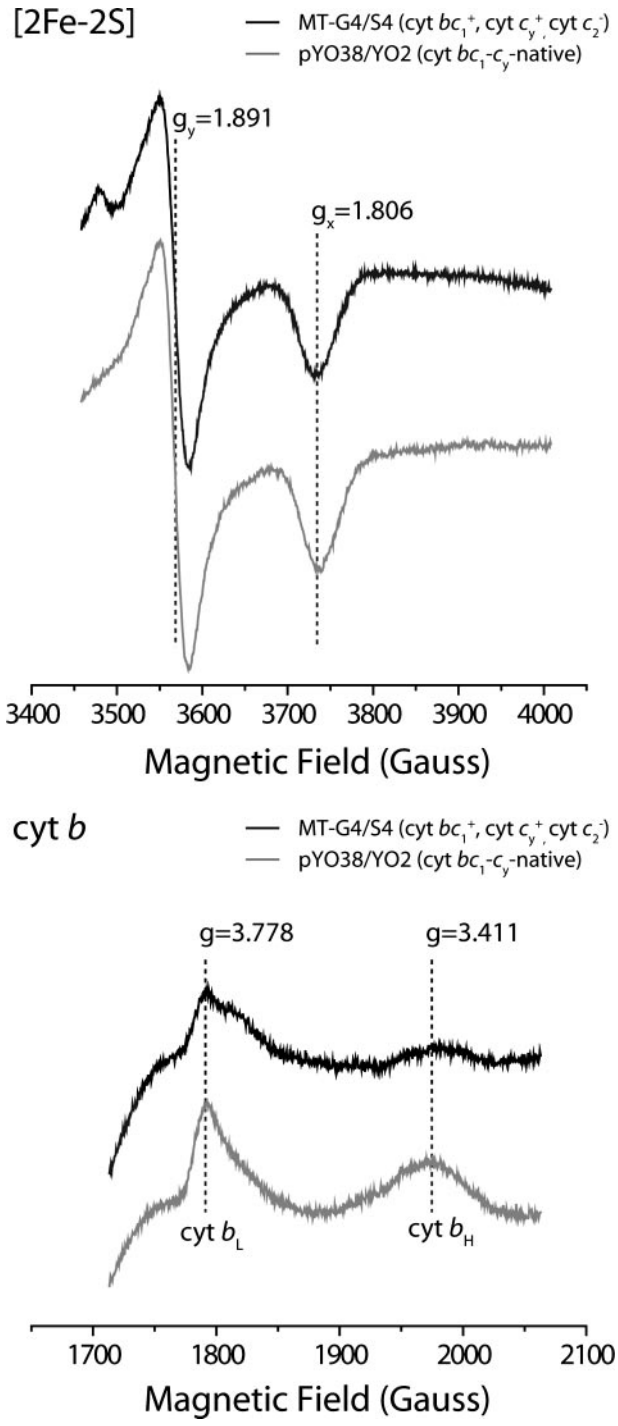

FIGURE 4. **EPR spectra of the cyt bc_1 complex [2Fe-2S] clusters (*upper panel*) and the cyt *b* hemes (*lower panel*) of *R. capsulatus* MT-G4/S4 lacking cyt c_2 and pYO38/YO2 containing a cyt bc_1-c_y fusion complex with a native cyt c_y linker, as described in the legend to Fig. 2.** For EPR spectroscopy of the [2Fe-2S] cluster or cyt *b* hemes (b_L and b_H), chromatophore membranes were reduced with ascorbate or air oxidized, respectively, as described in Refs. 35 and 36. Spectra were recorded at 20 K, 9.443 GHz, 12 G and 10 K, 9.59 GHz, 10 G temperature, microwave frequencies, and modulation amplitudes, respectively.

TABLE 2
Purification of the cyt bc_1-c_y fusion complex

Step	Protein	Total activity	Specific activity	Yield	-Fold
	mg	*units*[a]	*units/mg*	*%*	
Chromatophore + DDM	592				
Solubilized chromatophore	518	2,577	4.9	100	1.0
Q-Sepharose ff	33	634	19.3	25	3.9
FLAG	8[b]	204	27.2	8	5.5

[a] One unit of DBH_2-dependent cyt *c* reduction activity was defined as the amount of enzyme that produced 1 μmol of reduced cyt *c* per min under the assay conditions.
[b] FLAG-purified samples contained 70 and 87 nmol of cyt *c* (extinction coefficient, $\epsilon_{551-542}$ of 20 mM^{-1} cm^{-1}) and cyt *b* ($\epsilon_{560-574}$ of 28 mM^{-1} cm^{-1}) per milligram of protein, respectively.

DISCUSSION

In this work, first, we have characterized the physicochemical properties of a functional cyt bc_1-c_y complex that we constructed earlier (19) by fusing the COOH-terminal last amino acid of the cyt c_1 subunit of the cyt bc_1 complex to the NH_2-terminal first amino acid of its physiological membrane-bound electron acceptor cyt c_y (Fig. 1*A*). Using membrane preparations, detailed analyses demonstrated that the cyt bc_1-c_y fusion complex contained its prosthetic groups ([2Fe-2S] cluster and *b*- and *c*-type hemes) in appropriate amounts and assembled properly. Purification of the cyt bc_1-c_y fusion complex was needed to establish that it is an intact physical entity able to conduct membrane-confined Ps cyclic ET. This task was challenging because the fusion complex was susceptible to proteolytic degradation, and its chromatographic properties were distinct from the previously purified cyt c_y (10) and cyt bc_1 complexes (22). We developed a new procedure, using tandem Q-Sepharose ff ion-exchange and FLAG affinity column chromatographies, to obtain highly pure samples with good yields to initiate crystallization efforts. Unlike the dimeric cyt bc_1 complex, the purified cyt bc_1-c_y complex was a mixture of dimeric and tetrameric populations, with different oligomerization properties *in vitro*, possibly due to the presence of cyt c_y. The FLAG affinity purified samples contained small amounts of cyt c_1-c_y degradation products, running as an additional band around 30 kDa, and the Q-Sepharose column fractions were enriched in RC-LH subunits, usually absent in purified cyt bc_1 complexes (nLC-MS/MS data, not shown). During purification, although most of the Ps components are usually washed out from the cyt bc_1 complex in the presence of 0.01% DDM by a buffer of 0.2 M ionic strength, they remained with the cyt bc_1-c_y fusion complex. The significance, if any, of these apparent tighter associations remains to be seen.

Interestingly, both cyt *b* reduction and cyt *c* re-reduction rates exhibited by the cyt bc_1-c_y fusion complexes with shorter linkers were quasi-similar to those seen with strains harboring unconnected or fused cyt c_y and cyt bc_1 complexes with native cyt c_y linkers. These fast rates further evidenced that the monitored ETs were mediated by the membrane-bound cyts c_y, and not by their soluble versions (cyt S-c_y), somehow generated by proteolysis. Otherwise, as described in the accompanying work (38), the ET rates would have become much slower. Sharply contrasting the rates, the amplitudes of ET to the RCs were slightly smaller that the unconnected systems even in the presence of a cyt bc_1-c_y complex with a native cyt c_y linker, and became progressively smaller with shorter linkers. That only a fraction of all light-oxidized RC complexes can be reduced by cyt c_y has been well documented earlier using native systems (5, 12). This

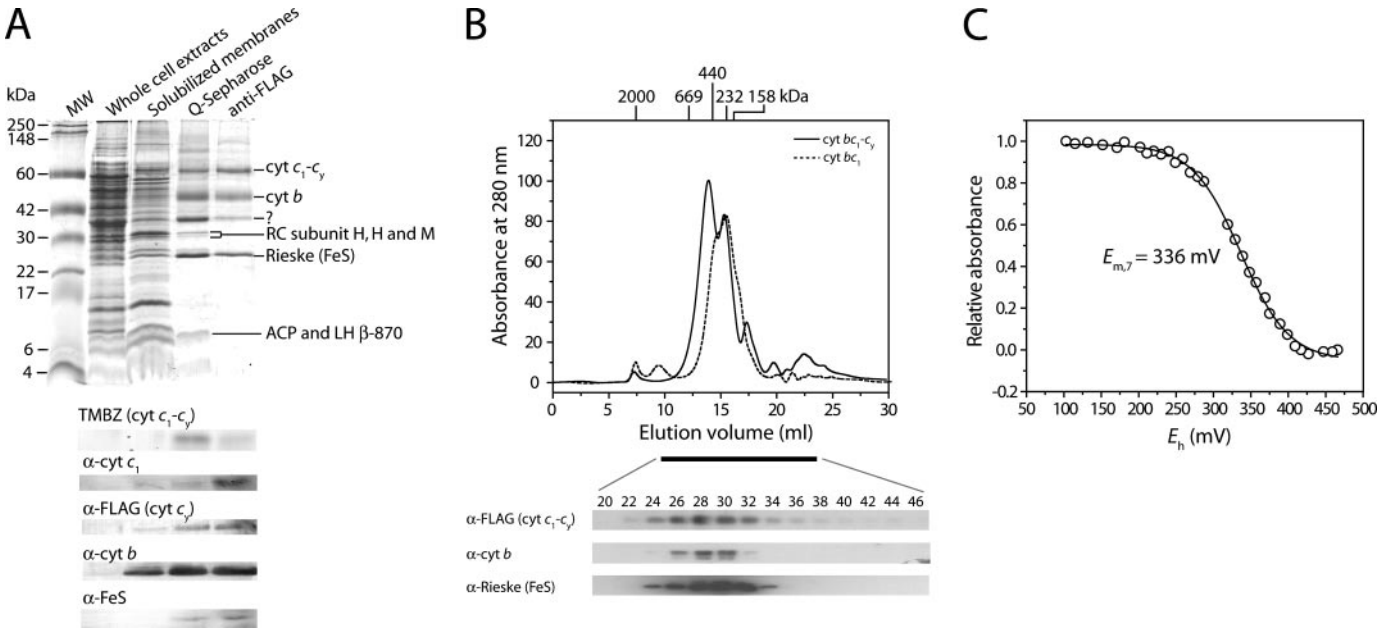

FIGURE 5. **Purification of the cyt bc_1-c_y fusion complex.** *A*, SDS-PAGE, TMBZ, and immunoblot analyses. Approximately 50 μg of total proteins per lane were used in each case, except the pool from anti-FLAG, which had only 10 μg. Column fractions obtained during the purification procedure, and α-cyt c_1, α-FLAG (*i.e.* cyt c_y), α-cyt *b*, and α-Fe-S antibodies were as described under "Experimental Procedures" and in the text. *B*, size exclusion chromatography (*upper panel*) of the purified cyt bc_1-c_y fusion complex and cyt bc_1 complex in the presence of 150 mM NaCl and 0.05% DDM. Gel filtration chromatography was performed using a Superose 6 HR 10/30 column, which was run at a flow rate of 0.3 ml/min, and the elution profile was monitored at 280 nm. The column was calibrated with blue dextran (2,000 kDa), thyroglobulin (669 kDa), apoferritin (440 kDa), catalase (232 kDa), and aldolase (158 kDa) as standards, run in the presence of 150 mM NaCl and 0.05% DDM, and their elution positions are indicated at the *top* of the chromatograph. Aliquots of each fraction (0.5 ml) were concentrated and subjected to 15% SDS-PAGE and immunoblot analyses (*lower panel*) using subunit-specific antibodies as described in *A*. *C*, dark equilibrium redox titration of the cyt c_1-c_y subunit of the purified cyt bc_1-c_y fusion complex (0.1 mg/ml). The titration was performed in 50 mM MOPS buffer (pH 7.0) containing 0.1 M KCl and 1 mM EDTA in the presence of 0.01% (w/v) DDM. Redox mediators were as described under "Experimental Procedures" (26). The $E_{m,7}$ value indicated was determined by fitting the normalized data to a $n = 1$ Nernst equation.

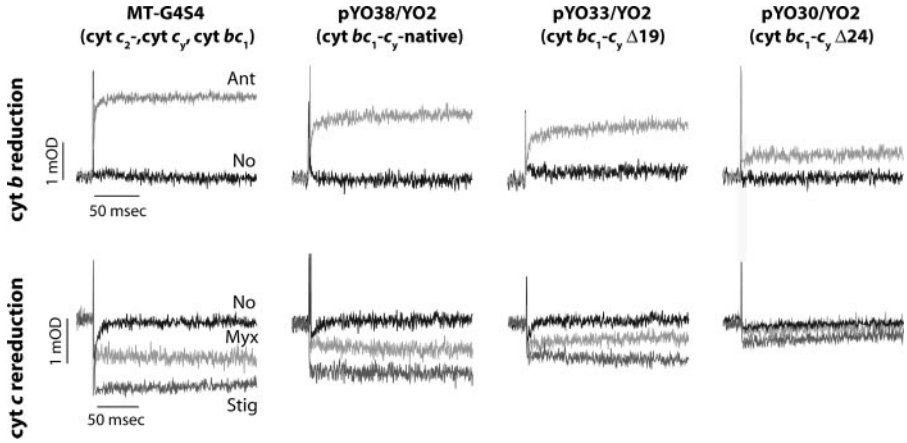

FIGURE 6. **Light-induced, time-resolved cyt *b* reduction and cyt *c* re-reduction kinetics of various *R. capsulatus* strains.** In each case, chromatophore membranes containing an amount of RC equal to 0.45 μM were resuspended in 50 mM MOPS buffer (pH 7.0) containing 100 mM KCl and 100 mM EDTA at an E_h of 100 mV. The amount of RC was determined based on the extent of its photooxidation by a train of 10 flashes separated by 50 ms at an E_h of 380 mV, and using an extinction coefficient $\epsilon_{605\text{-}540}$ of 29 mM^{-1} cm^{-1}, as described under "Experimental Procedures." The traces for cyt *b* reduction (*upper panel*) were monitored in the absence (*No*) and the presence of the Q_i site inhibitor antimycin (*Ant*, 5 μM), and those for cyt *c* re-reduction (*lower panel*) were in the absence of inhibitor or in the presence of myxothiazol (*Myx*, 5 μM), where no QH_2 oxidation takes place at the Q_o site, or in the presence of stigmatellin (*Stig*, 1 μM), where no electron is transferred from the [2Fe2S] cluster to the c_1 heme. All samples contained the same amounts of the cyt bc_1-c_y complexes as documented in Figs. 2 and 3.

work therefore demonstrated that the amounts of electronically coupled RC-LH-cyt bc_1-c_y fusion complexes diminished further with shorter cyt c_y linkers, reflecting the distance dependence of efficient cyclic electron transport between the donor and acceptor complexes in Ps membranes. Furthermore, the progressive decrease suggested that membranes might contain a distribution of such closely associated photosynthetic units.

Even though the cyt bc_1-c_y fusion complexes with shorter cyt c_y linkers were produced in comparable amounts irrespective of the linker sizes, they supported Ps growth at different degrees. Comparison of the shortest (Δ24-c_y) and barely functional cyt c_y linker with that of non-Ps competent *R. sphaeroides* cyt c_y, which is 26 residues shorter than that of its *R. capsulatus* counterpart (Fig. 1*A*), suggested that at least a linker of about 44–46 amino acids long (provided that the native linker is about 70 residues long) is required to couple electronically the cyt bc_1-c_y fusion complex and the RC surrounded with its LH complexes. Assuming that both the RC (30) and the cyt bc_1 complex (31) extend into the periplasm by ~30 Å, then half of the remaining linker would be consumed to bring the cyt *c* domain of cyt c_y to the same plane

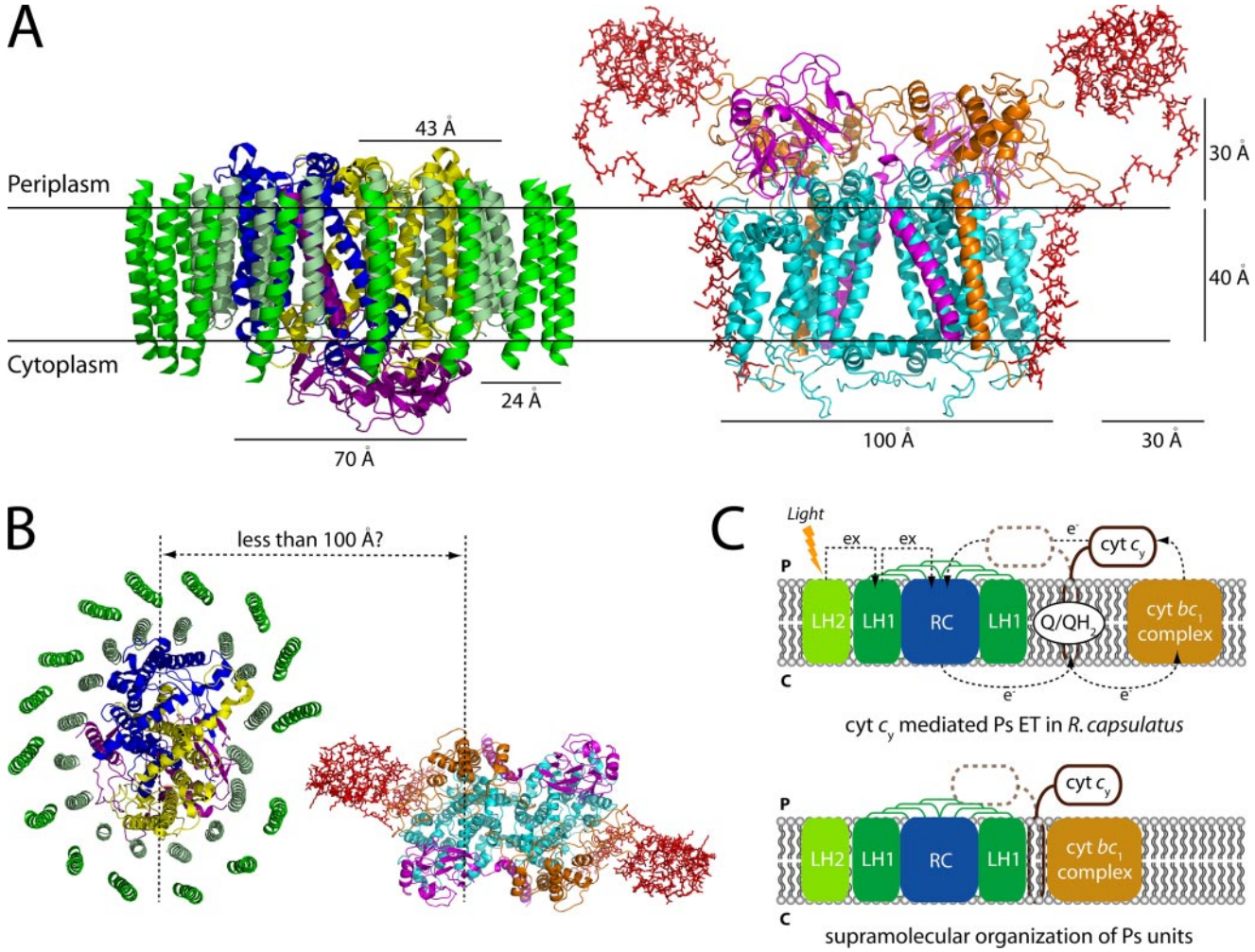

FIGURE 7. *A*, crystal structure of the RC-LH1 core complex (PDB 1PYH) from *Rhodopseudomonas palustris* and hypothetical three-dimensional structural model of *R. capsulatus* cyt bc_1-c_y fusion complex (pYO30/YO2, Δ24-c_y) (with the transmembrane helices of cyt bc_1 shown as *ribbons*, and cyt c_y (Δ24-c_y) shown as *sticks*), are drawn using the program PyMOL. The narrow section of the RC (subunits L, *yellow*; *M*, *blue*; *H*, *purple*) surrounded by the LH1 complex (chains α, *pale green* and β, green) and the cyt bc_1-c_y fusion complex (subunits cyt *b*, *cyan*; cyt c_1, *orange*; cyt c_y, *red*; and the Fe-S protein, *magenta*) are viewed parallel to the membrane plane. *B*, top view (perpendicular to the membrane plane) of the RC-LH1 core complex and the cyt bc_1-c_y fusion complex with the shortest cyt c_y linker (Δ24-c_y) is shown. Note that to reach the central part of RC subunits L and M in the RC-LH1 and cyt bc_1-c_y fusion complexes, the cyt c domain of cyt c_y (assuming that its linker is stretched out in a fashion parallel to the membrane) needs to reach out for about 100 Å. *C*, a schematic representation of the major membrane proteins involved in cyclic ET of purple bacterial photosynthesis (*upper panel*), and a proposed mechanism for cyt c_y-mediated cyclic ET via supraorganization of *R. capsulatus photosynthetic unit* (*lower panel*). *cyt bc_1 complex*, hydroquinone cyt *c* oxidoreductase; *cyt c_y*, membrane-associated cytochrome c_y. *Arrows* indicate directions of electron (e^-) and excitation (*ex*) flows.

with its physiological partners. The remaining 20–25-residue long linker controlling its electronic coupling ability then suggest that the RC-LH complexes and the cyt bc_1-c_y complex must be very close to each other, possibly forming large structural complexes. Furthermore, it is noteworthy that both the *R. sphaeroides* cyt c_y (9) and *R. capsulatus* cyt bc_1-c_y fusion complexes with shorter linkers convey electrons to their cognate cyt *c* oxidases.[5] Thus, Ps supercomplexes apparently require longer cyt c_y linkers than the respiratory counterparts, possibly due to the LH complexes surrounding the RCs.

Kinetic behaviors of functional supercomplexes in *R. sphaeroides* Ps membranes between the RC and the "trapped" cyt c_2 acting in a locally confined manners (14, 32–34), strongly suggest that the RC-LH and the cyt bc_1 complexes must be very close to each other. The data presented here provide complementary structural and kinetic information for such Ps supercomplexes, with a ratio of the RC-LH:cyt bc_1:cyt c_2 (or c_y) being 2:1:1 (13, 33). Joliot *et al.* (33) proposed that in the RC-LH complexes dimerized via LH-PufX interactions, two RC dimers interact with a single cyt bc_1 complex dimer. If this is also the case with the cyt bc_1-c_y fusion complexes in the Ps membranes, then c_y cyts might be located between the cyt bc_1 complexes and the RC-LH complexes with their membrane anchors in the vicinity of the quasi-closed LH rings, promoting tighter associations between the Ps components. The motion constraints thus imposed on cyt c_y might then only be compensated by a linker long enough to allow its movement between the cyt bc_1 complex dimers and the opposing RC-LH complexes of *R. capsulatus* (Fig. 7).

In summary, the availability of functional cyt bc_1-c_y complexes with shorter linkers affecting the coupling to the RC-LH complexes now provide compelling indications that hardwired

[5] Y. Öztürk, D. Zannoni, and F. Daldal, unpublished data.

Ps units occur in membranes. Future purification of these Ps units will initiate studies addressing how the membrane supercomplexes are formed and regulated *in vivo* in response to changing environmental conditions, and why some organisms contain both a soluble cyt c_2 and a membrane-anchored cyt c_y.

Acknowledgments—We thank C. Sanders for helpful discussions and O. Onder and N. Selamoglu for mass spectrometry analyses.

REFERENCES

1. Berry, E. A., Guergova-Kuras, M., Huang, L. S., and Crofts, A. R. (2000) *Annu. Rev. Biochem.* **69,** 1005–1075
2. Darrouzet, E., Cooley, J. W., and Daldal, F. (2004) *Photosynth. Res.* **79,** 25–44
3. Crofts, A. R., and Meinhardt, S. W. (1982) *Biochem. Soc. Trans.* **10,** 201–203
4. Gennis, R. B., Barquera, B., Hacker, B., Van Doren, S. R., Arnaud, S., Crofts, A. R., Davidson, E., Gray, K. A., and Daldal, F. (1993) *J. Bioenerg. Biomembr.* **25,** 195–209
5. Jenney, F. E., Jr., and Daldal, F. (1993) *EMBO J.* **12,** 1283–1292
6. Zannoni, D., and Daldal, F. (1993) *Arch. Microbiol.* **160,** 413–423
7. Jenney, F. E., Jr., Prince, R. C., and Daldal, F. (1994) *Biochemistry* **33,** 2496–2502
8. Donohue, T. J., McEwan, A. G., Van Doren, S., Crofts, A. R., and Kaplan, S. (1988) *Biochemistry* **27,** 1918–1925
9. Myllykallio, H., Zannoni, D., and Daldal, F. (1999) *Proc. Natl. Acad. Sci. U. S. A.* **96,** 4348–4353
10. Myllykallio, H., Jenney, F. E., Jr., Moomaw, C. R., Slaughter, C. A., and Daldal, F. (1997) *J. Bacteriol.* **179,** 2623–2631
11. Schoepp-Cothenet, B., Schutz, M., Baymann, F., Brugna, M., Nitschke, W., Myllykallio, H., and Schmidt, C. (2001) *FEBS Lett.* **487,** 372–376
12. Jenney, F. E., Jr., Prince, R. C., and Daldal, F. (1996) *Biochim. Biophys. Acta* **1273,** 159–164
13. Myllykallio, H., Drepper, F., Mathis, P., and Daldal, F. (1998) *Biochemistry* **37,** 5501–5510
14. Vermeglio, A., and Joliot, P. (1999) *Trends Microbiol.* **7,** 435–440
15. Eubel, H., Jansch, L., and Braun, H. P. (2003) *Plant Physiol.* **133,** 274–286
16. Schagger, H., and Pfeiffer, K. (2000) *EMBO J.* **19,** 1777–1783
17. Hackenbrock, C. R., Chazotte, B., and Gupte, S. S. (1986) *J. Bioenerg. Biomembr.* **18,** 331–368
18. Crofts, A. R. (2000) *Trends Microbiol.* **8,** 105–106
19. Lee, D. W., Ozturk, Y., Mamedova, A., Osyczka, A., Cooley, J. W., and Daldal, F. (2006) *Biochim. Biophys. Acta* **1757,** 346–352
20. Atta-Asafo-Adjei, E., and Daldal, F. (1991) *Proc. Natl. Acad. Sci. U. S. A.* **88,** 492–496
21. Daldal, F., Cheng, S., Applebaum, J., Davidson, E., and Prince, R. C. (1986) *Proc. Natl. Acad. Sci. U. S. A.* **83,** 2012–2016
22. Valkova-Valchanova, M. B., Saribas, A. S., Gibney, B. R., Dutton, P. L., and Daldal, F. (1998) *Biochemistry* **37,** 16242–16251
23. Smith, P. K., Krohn, R. I., Hermanson, G. T., Mallia, A. K., Gartner, F. H., Provenzano, M. D., Fujimoto, E. K., Goeke, N. M., Olson, B. J., and Klenk, D. C. (1985) *Anal. Biochem.* **150,** 76–85
24. Laemmli, U. K. (1970) *Nature* **277,** 680–685
25. Thomas, P. E., Ryan, D., and Levin, W. (1976) *Anal. Biochem.* **75,** 168–176
26. Dutton, P. L. (1978) *Methods Enzymol.* **54,** 411–435
27. Robertson, D. E., Ding, H., Chelminski, P. R., Slaughter, C., Hsu, J., Moomaw, C., Tokito, M., Daldal, F., and Dutton, P. L. (1993) *Biochemistry* **32,** 1310–1317
28. Darrouzet, E., Moser, C. C., Dutton, P. L., and Daldal, F. (2001) *Trends Biochem. Sci.* **26,** 445–451
29. Darrouzet, E., Valkova-Valchanova, M., Moser, C. C., Dutton, P. L., and Daldal, F. (2000) *Proc. Natl. Acad. Sci. U. S. A.* **97,** 4567–4572
30. Roszak, A. W., Howard, T. D., Southall, J., Gardiner, A. T., Law, C. J., Isaacs, N. W., and Cogdell, R. J. (2003) *Science* **302,** 1969–1972
31. Berry, E. A., Huang, L. S., Saechao, L. K., Pon, N. G., Valkova-Valchanova, M., and Daldal, F. (2004) *Photosynth. Res.* **81,** 251–275
32. Jungas, C., Ranck, J. L., Rigaud, J. L., Joliot, P., and Vermeglio, A. (1999) *EMBO J.* **18,** 534–542
33. Joliot, P., Joliot, A., and Vermeglio, A. (2005) *Biochim. Biophys. Acta* **1706,** 204–214
34. Joliot, P., Vermeglio, A., and Joliot, A. (1989) *Biochim. Biophys. Acta* **975,** 336–345
35. Darrouzet, E., Valkova-Valchanova, M., and Daldal, F. (2000) *Biochemistry* **39,** 15475–15483
36. Cooley, J. W., Ohnishi, T., and Daldal, F. (2005) *Biochemistry* **44,** 10520–10532
37. Gray, K. A., Dutton, P. L., and Daldal, F. (1994) *Biochemistry* **33,** 723–733
38. Öztürk, Y., Lee, D.-W., Mandacı, S., Osyczka, A., Prince, R. C., and Daldal, F. (2008) *J. Biol. Chem.* **283,** 13964–13972